Nanocrystalline and amorphous surface structure of 0.45%C steel produced by high current pulsed electron beam

Q. F. GUAN*, P. L. YANG
Department of Material Science and Engineering and State Key Laboratory for Superhard Materials, Jilin University, Changchun 130025, People's Republic of China
E-mail: guanqingfeng@jlu.edu.cn

H. ZOU
College of Science, Civil Aviation University of China, Tianjin 300300, People's Republic of China

G. T. ZOU
State Key Laboratory for Superhard Materials, Jilin University, Changchun 130025, People's Republic of China

Published online: 12 January 2006

We study in this article the microstructure and phase transformation on the near-surface of 0.45% C carbon steel during the high current pulsed electron beam processing by using electron microscopy. Based on a physical model, the temperature profile is simulated for carbon steel. The depth of heat-affected zone, the initial melting position, heating rate and quenching rate are computed. The original crystalline structure was changed to a different degree that grew with the numbers of bombardment, and in the near-surface layer amorphous states and nanocrystaline structures consisting of grains of γ-phase and cementite were formed after multiple pulses.

1. Introduction

It is known that most failures of engineering materials are very sensitive to the structure and properties of material surface, and in most cases material failures occur on the surface. Therefore, optimization of surface structure and properties may effectively improve the global behavior of material [1]. With the increasing evidences of unique properties for nanostructured and amorphous materials, it is reasonably expected to achieve surface modification by generation of a nanostructured and/or amorphous surface layer [2–4].

Recently, the application of high-current pulsed electron beam (HCPEB) is becoming of increasing interest to material processing [5–7]. It is characterized by a high power density of 10^8–10^9 W/cm^2 at the target surface. During the interaction of incident pulsed electron beam with the surface of materials, such a high energy is deposited only in a very thin layer within a short time and causes superfast processes such as heating, melting, and evaporation, followed by superfast solidification of material. The dynamic stress fields induced in these processes cause intense deformation processes in the material and lead to significant modification effects in the material. As a result, metastable structure-phase states may appear in the surface layers, which are capable of providing improved physical, chemical and strength properties of the material unattainable with conventional surface treatment techniques [5]. In this paper, we report the formation of a nanostructure and amorphous structure in the surface layer of a 0.45% C carbon steel by using the HCPEB surface treatment. The temperature profile is also simulated for substrate of carbon steel.

2. Experimental procedures

A schematic diagram of the HCPEB source (Nadezhda-2) is given in Fig. 1. It produces an electron beam of low energy (10–40 KeV), high peak current (10^2– 10^3 A/cm^2), short pulsed duration of about 1 μs, and high efficiency (repeating pulse interval being 10 s). The electron beam

*Author to whom all correspondence should be addressed.
0022-2461
DOI: 10.1007/s10853-005-2463-0

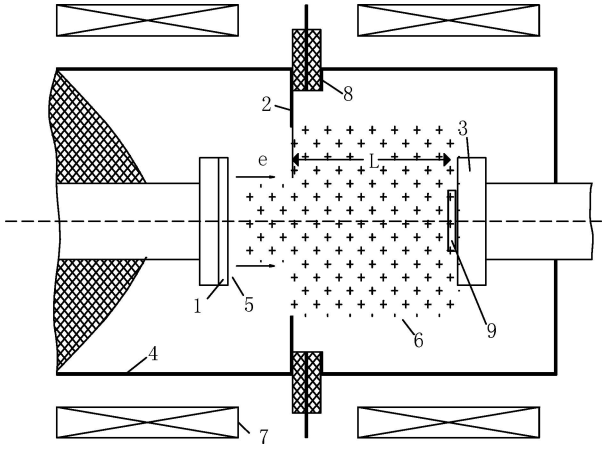

Figure 1 Schematic diagram of the HCPEB source using plasma filled systems based on vacuum spark plasma. (1) cathode, (2) anode, (3) collector, (4) vacuum-chamber, (5) cathode plasma, (6) anode plasma, (7) solenoid, (8) spark source, (9) specimen.

is generated by an explosive emission cathode. The cathode-target distance and the energy control the beam energy density and hence the treatment effects. The HCPEB source has been reported in our previous work [6]. For more details about the HCPEB system, the readers are referred to Proskurovsky *et al*. [5, 7].

An annealed 0.45%C steel, contained (mass, %) 0.45C, 0.31Si, 0.58 Mn, 0.010 P, 0.018 S and remainder Fe, was selected as the target material. Specimens were machined to size 14 mm in length, 10 mm in width, and 10 mm in height, and one side surface was mirror polished. The bombardment of samples were carried out using HCPEB under the following conditions: electron energy was 28 KeV, the current pulsed duration was 3.5 μs, energy density was 4 J cm^{-2} and the pressure of residual gas in the vacuum chamber was about 10^{-5} Torr. The specimens were bombarded 1, 5 and 10 pulses, respectively.

Microstructural examinations were performed with a scanning electron microscope (SEM) of type JSM-5310 and a transmission electron microscope (TEM) of type H-800. The foils used to TEM observations were obtained by preparing one-sided mechanically prethinned, dimpled and, in the last step, electrolytical thinning of the thin plates until the electron transparency occurred. The depth of the analyzed near-surface layer was about 0.5–1.5 μm.

3. Results and discussion

3.1. Numerical simulations

The temperature field $T(x, t)$ can be calculated by solving a one-dimensional thermal conductivity equation [5, 8, 9]

$$\rho c \frac{\partial T(x,t)}{\partial t} = \frac{\partial}{\partial x}\left(k(T)\frac{\partial T(x,t)}{\partial x}\right) + g(x,t) + L \quad (1)$$

where ρ the mass density, $c(T)$ the specific heat, $k(T)$ the thermal conductivity, $g(x, t)$ the power absorption per unit volume, and L the latent heat per unit mass (in J/kg). The thermal conductivity k and specific heat c are intrinsic properties of the material and functions of the temperature T [10, 11]. In our numerical simulation, we adopt the equivalent heat quantity method, i.e., the absorbed and released latent heats per unit volume are converted into temperature compensationsΔT, which is proportional to L, the latent heat,

$$\Delta T = \frac{L}{c} \quad (2)$$

The power absorption per unit volume can be expressed as [12]

$$g(x,t) = \eta_A \frac{Uj}{r} f(x,r) = \eta_A \frac{P(t)}{Sr} f(x,t) \quad (3)$$

where $j = j(t)$ is the electron current density, U the acceleration voltage, $P(t)$ the power of electron beam, S the irradiation area of the electron beam, h α the absorption rate of the impinging beam power (being 0.8 and 0.7, respectively, for A1 and Cu ~ref. 15) and $f(x, r)$ the distribution function of the absorbed power density over the electron range in the target which can be described by [12]

$$f(x,r) = 1 - \frac{9}{4}\left(\frac{x}{r} - \frac{1}{3}\right)^2, \quad (4)$$

as well as $r(t)$ the electron range in the target calculated from the formula [12]

$$r \approx 2.1 \times 10^{-5} \frac{U^2}{\rho}, \quad 10\,\text{kV} \le eU \le 100\,\text{keV} \quad (5)$$

where the units are kV for U, kg m^{-3} for ρ, and μm for r.

The coefficient of temperature conductivity is defined with a relation $\alpha = k/\rho\, c$, where α increases as the thermal conductivity of the material increases and the specific heat decreases. The coefficient of temperature conductivity of carbon steel is approximately 1.4×10^{-5} m^2/s in room temperature [10]. In the present numerical simulations, we used the following parameters: the electron energy 28 keV, the pulse duration 0.8 μs, and the total deposited energy density per pulse 4.0 J/cm^2.

Fig. 2 gives the temperature distributions of carbon steel over a depth range of 0–40 μm and a time range of 0–2 μs. The near-top flat areas of the profile are the melting plateau of the 0.45% carbon steel at about 1537°C. From Fig. 2, we can clearly see that the depth of heat-affected zone of the carbon steel is below 10 μm. Otherwise, the melting starts from 0.6 μs and the site is at a sublayer about 0.25 μm from the surface. The heating rate $\approx 10^8$ K/s and the cooling rate $\approx 10^6$ K/s.

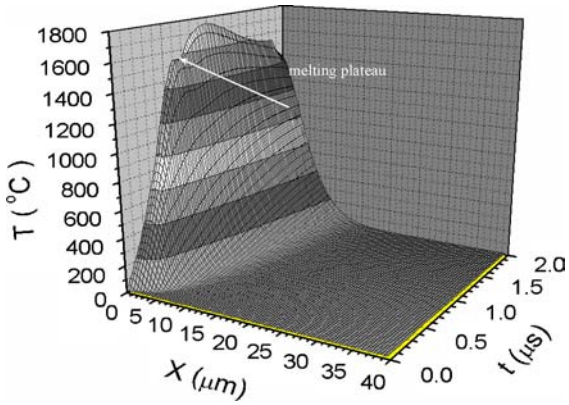

Figure 2 Temperature distribution of carbon steel at different position and time.

3.2. Surface microstructure

As we know, untreated sample possess typical pearlite microstructure consisting of laminated cementite and α-ferrite, as shown in Fig. 3a. After irradiation with 4 J/cm^2, few cementites were observed in the near- surface. In Fig. 3b (cross-section), the cementites almost disappeared in the zone approximately 10 μm away from the surface. It is in a good agreement with the numerical results. It is revealed that the cementites underwent dissolution during HCPEB treatment. This result suggests that a supersaturated Fe (C) solid solution

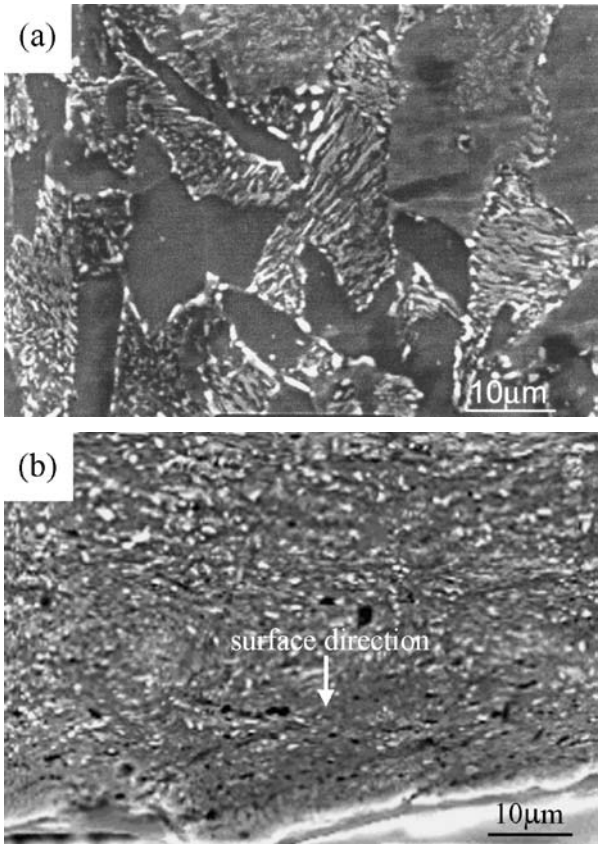

Figure 3 Showing the cross-section SEM images of 0.45% C steel. (a) untreated, (b) after 1-pulse HCPEB irradiation.

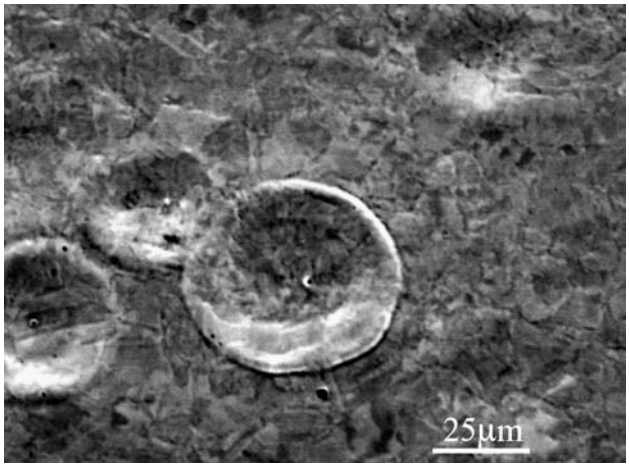

Figure 4 A typical crater image in the surface of the 0.45% carbon steel treated with 1-pulse at 28 kV.

phase was formed in the near-surface during a rapid solidification process generated due to HCPEB treatment.

Fig. 4 (top view) reveals that the irradiated surface of 0.45%C steel has melted and many craters were formed. They appear homogeneously over the irradiated surface. Based on the results of numerical results, such a typical morphology is the result of the local sublayer melting and eruption through the solid outer surface.

TEM micrographs of samples near-surface under various pulse bombardments are shown in Figs. 5–7, respectively. Fig. 5a shows the typical pearlite microstructure of untreated sample consisting of laminated cementite and α-ferrite. After 1 pulse treatment of HCPEB, the cementite phase was partly dissolved and the dislocation cell structure was formed in α-phase, as shown in Fig. 5b. This is the signature of severe stress and plastic deformation caused by rapid heating and solidification. It suggests that severe stresses were induced and the stresses cause the dislocations tangling tempestuously each other and finally forming the dislocation cell structure during HCPEB treatment.

After 5 pulses, the laminated cementite phase almost disappeared, whereas the nanostructures were formed, as shown in Fig. 6a. Corresponding selected area electron diffraction (SAED) pattern (Fig. 6b) reveals that the diffraction rings induced by nanostructure are due to the both austenite and cementite types of nanostructure particles. The stronger diffraction spots can be indexed by α-ferrite. It suggests that nanograined austenite and cementite precipitate in the ferrite matrix. The nanostructure particle size in Fig. 6a can be estimated directly. It ranges from about 5 to 15 nm.

The surface structures of a 0.45%C steel with low energy, high current electron beams have already been investigated by Proskurovsky *et al*. [5]. They reported that layer-by-layer TEM examination has shown that a graded structure is formed in the heat affect zone (HAZ), and in the near-surface layer quenched from melt a nanocrystalline structure consisting of grains of α-ferrite and

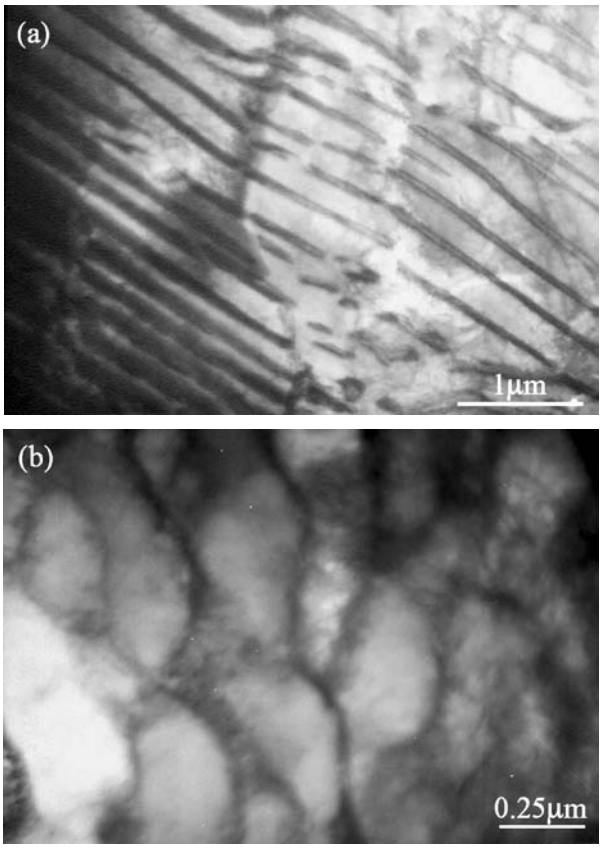

Figure 5 (a) TEM images of the original sample, (b) the near surface zone of the 0.45% carbon steel treated with 1-pulse.

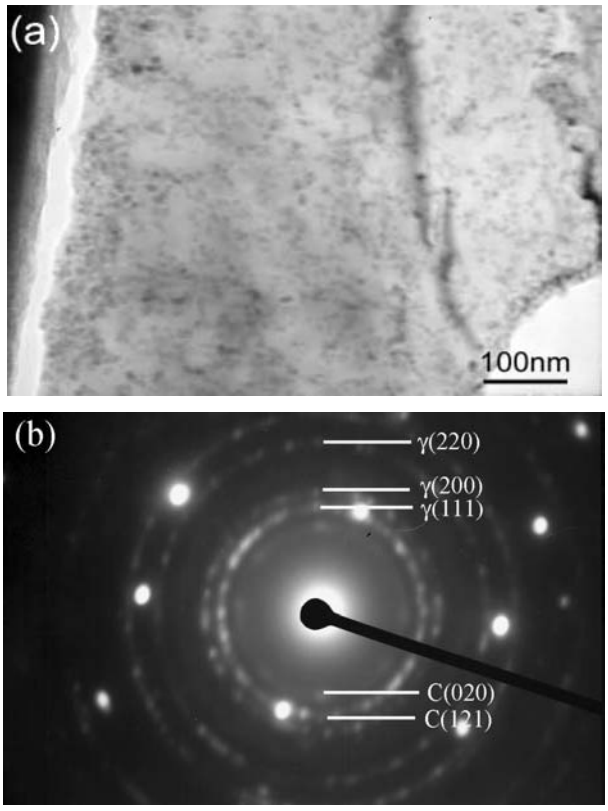

Figure 6 (a) TEM bright field image showing nanograined cementite and austenite in ferrite matrix in the specimen treated by 5-pulses at 4 J/cm^2, (b) the corresponding electron diffraction pattern.

γ-austenite phase and containing no martensite crystals is formed. As compared with the Proskurovsky's work, the carbide type and γ-austenite phase of nanocrystalline and no α-ferrite structure of nanostructured particles were observed. The martensite crystals were still absent. This fact may be interpreted in view of dependence of the temperature A_{c3} on the rate of heating of the target. As we know, the higher is the heating rate, the higher the temperature A_{c3}. From Fig. 1 it follows that for our case (heating rate $\approx 10^8$ K/s) the temperature A_{c3} is about 400 K higher than the equilibrium A_{c3} temperature [10]. Thus, this appears to be the real reason of martensite absence.

After 10-pulses irradiation, the austenite and carbide types of nanostructure particles were still observed, and these particles seem to have even smaller size comparing with that of 5-pulse bombardments. It suggests that the particle size decrease gradually with increasing the pulse bombardments of HCPEB. The reason of the particle size decrease retains unclear. It appears to be attributed to the subsequent bombardment of HCPEB induced higher internal compressive stress, which restricts the growth of nanostructure particles under subsequent cooling process. Whereas, the annealing effect is minor due to the superfast cooling rate (about 10^6 K/s).

Besides the nanostructure particles, it is interesting that amorphous structure was also massively formed in the case of 10-pulses. Fig. 7a shows the TEM bright field image of amorphous structure. The corresponding SAED pattern is shown in Fig. 7b, which exhibits typical diffraction rings of amorphous structure. However, the amorphous structure is not observed in the samples treated with 1 and 5 pulses. It appears to be interpreted by using the viewpoint of size effects of nanostructure material [13]. According to this viewpoint, the formation of the amorphous may be attributed to the size of some nanostructure particles formed as above-mentioned mechanism in local zones below a critical crystal size. Free energy simulations of nanostructure material and related glass suggest that a phase transition from the nanocrystalline state to the glass should occur below a critical grain size [14]. In this case, nanostructure materials are unstable relative to the amorphous as they exhibit a higher free energy.

It is believed that amorphization of the Fe-C alloys has never been achieved by rapid quenching as far as we know. Thus, the rapid solidification seems not to be sole reason for the formation of the amorphous phase during HCPEB treatments, although the quenching rate could reach 10^8 K/s. When an electron irradiated target, due to the drastic temperature change, a steep temperature gradient is generated along the incident direction of the beam. However, the thermal expansion in the directions vertical to the beam is strongly resisted, causing the surface thermal stress. When material was subjected to a HCPEB irradiation, a mass of structure defects were induced in the near-surface of the target. The stress induced by subsequent irradiations is coupled with these structure defects formed before to harden the target. Therefore, the thermal expansion due to the lateral

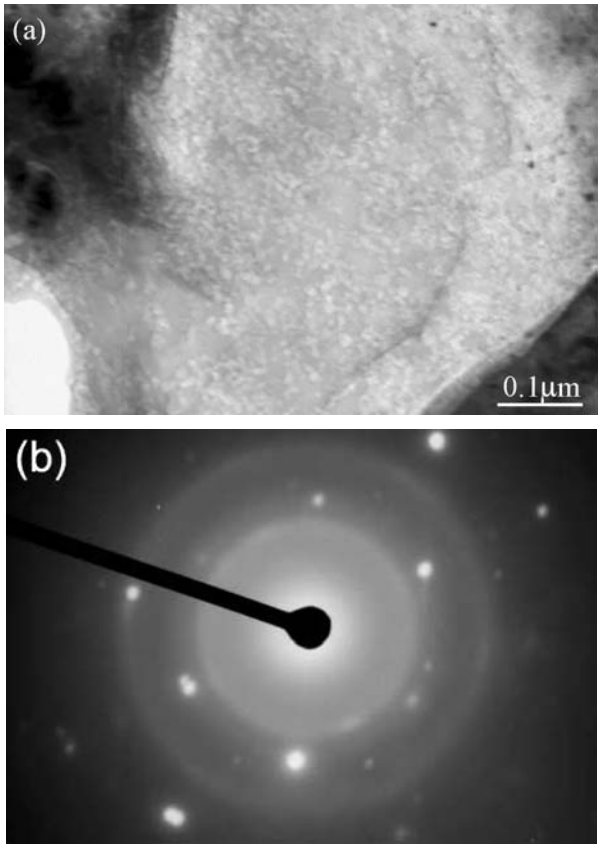

Figure 7 (a) TEM bright field image of the amorphous structure of the sample treated by 10-pulses at 4 J/cm^2, (b) the corresponding electron diffraction pattern, the stronger diffraction spots can be indexed by α-ferrite.

confinement along the surface becomes even stronger with increasing the pulse number. Thus, higher values of the stress are achieved in the case of multiple pulses. This external force may be increased internal stress to an extraordinarily high level. The numerical simulation of the thermal-mechanical process of HCPEB treatment by Zou *et al*. [15] suggests that the quasistatic stress is coupled with the temperature field and the maximum compressive stress in the near surface layer reaches several hundreds of MPa after multiple pulses, which can produce very violent deformation in the surface layer of the irradiated material. Under such high stress, all atom of the irradiated surface layer rather than only the atom near the core of dislocation are brought to the condition to displace during the deformation. The natural expectation is the formation of larger zones containing disorder atom in it, just like the atom near the core of dislocation and/or grain boundary. The nanostructure and the amorphous mentioned above may be an implication.

4. Conclusions

The initial samples of 0.45%C steel was treated by HCPEB with an energy range of 28 kV. Surface structures were studied using SEM and TEM. Based on a physical model, the temperature profile is simulated for carbon steel. According to experimental and numerical results, we conclude as follows:

The depth of heat-affected zone of the carbon steel is below 10 μm. The melting starts from 0.6 μs and the site is at a sublayer about 0.25 μm from the surface. The heating and quenching rate is approximately 10^8 and 10^6 K/s, respectively. After HCPEB post treatments, a supersaturated Fe (C) solid solution phase was formed in the near-surface. Rapid heating and solidification induced heavy plastic deformation, which caused the formation of the dislocation cells by 1-pulse bombardment. After multi-pulse bombardments, both austenite and carbide types of nanostructure particles were formed from the supersaturated Fe (C) solid solution phase. After 10-pulses bombardments, besides austenite and carbide types of nanostructure particles, additional amorphous structure was formed in the local zones. The supersaturated carbon solution in the parent ferrite phase due to dissolution of cementite is the origin of the nanostructured formation.

References

1. K. LU, J. T. WANG and W. D. WEI, *J. Appl. Phys.* **69** (1991) 522.
2. U. ERB, A. M. EL-SHERIK, G. PALUMBO and K. T. AUSU, *Nanostruct. Mater.* **2** (1993). 383.
3. A. E. BERKOWITZ and J. L. WALTER, *J. Mater. Res.* **2** (1987) 277.
4. R. NAGARAJAN and K. CHATTOPADHYAY, *Acta Metall. Mater.* **42** (1994) 947.
5. D. I. PROSKUROVSKY, V. P. ROTSHTEIN and G. E. OZUR, *J. Vac. Sci. Technol.* **A16** (1998) 2480.
6. Q. F. GUAN, L. PAN, H. ZOU, A. M. WU, S. Z. HAO, Q. Y. ZHANG, C. DONG and G. T. ZOU, *J. Mater. Sci.* **39** (20) 6349.
7. D. I. PROSKUROVSKY, V. P. ROTSHTEIN and G. E. OZUR, *Surf. Coat. Technol. 125,* **49** (2000) **6**.
8. A. B. MARKOV and V. P. ROTSHTEIN, *Nucl. Instrum. Methods Phys. Res. B* **132** (1997) 79.
9. A. D. POGREBNJAK, S. BRATUSHKA and V. I. BOYKO, *ibid.* **145** (1998) 373.
10. Metals Research Association of China, "Handbook of Physical Properties of Metallic Material", (Metallurgical Industry Press, Beijing 1987), Vol. 1, p. 263 (in Chinese).
11. G. J. ZHU, "Engineering Heat and Mass Transfer" (Aviation Industry Press: Beijing 1989), p. 571 (in Chinese).
12. S. SCHILER, U. HEISIG and S. PANZER, "Electron Beam Technology" (Wiley- Interscience German Democratic Republic, 1982), pp. 29–42.
13. H. GLETTER, *Acta Mater.* **48** (2000) 1.
14. D. WOLF, D. WANG, S. PHILLPOT and H. GLETTER, *Phil. Lett. A* **73** (1996) 517.
15. J. X. ZOU, Y. QIN, C. DONG, X. G. WANG, A. M. WU and S. Z. HAO, *J. Vac. Sci. Technol.* **A22** (2004) 545.

Received 13 December 2004
and accepted 23 May 2005